Cross section and transverse single-spin asymmetry of muons from open heavy-flavor decays in polarized $p+p$ collisions at $\sqrt{s}=200$ GeV

C. Aidala,[39,43] N. N. Ajitanand,[61,*] Y. Akiba,[56,57,†] R. Akimoto,[12] J. Alexander,[61] M. Alfred,[24] K. Aoki,[32,56] N. Apadula,[29,62] H. Asano,[35,56] E. T. Atomssa,[62] T. C. Awes,[52] C. Ayuso,[43] B. Azmoun,[7] V. Babintsev,[25] A. Bagoly,[17] M. Bai,[6] X. Bai,[11] B. Bannier,[62] K. N. Barish,[8] S. Bathe,[5,57] V. Baublis,[55] C. Baumann,[7] S. Baumgart,[56] A. Bazilevsky,[7] M. Beaumier,[8] R. Belmont,[13,67] A. Berdnikov,[59] Y. Berdnikov,[59] D. Black,[8] D. S. Blau,[34] M. Boer,[39] J. S. Bok,[50] K. Boyle,[57] M. L. Brooks,[39] J. Bryslawskyj,[5,8] H. Buesching,[7] V. Bumazhnov,[25] C. Butler,[21] S. Butsyk,[49] S. Campbell,[14,29] V. Canoa Roman,[62] C.-H. Chen,[57] C. Y. Chi,[14] M. Chiu,[7] I. J. Choi,[26] J. B. Choi,[10,*] S. Choi,[60] P. Christiansen,[40] T. Chujo,[66] V. Cianciolo,[52] B. A. Cole,[14] M. Connors,[21,57] N. Cronin,[44,62] N. Crossette,[44] M. Csanád,[17] T. Csörgő,[18,69] T. W. Danley,[51] A. Datta,[49] M. S. Daugherity,[1] G. David,[7] K. DeBlasio,[49] K. Dehmelt,[62] A. Denisov,[25] A. Deshpande,[57,62] E. J. Desmond,[7] L. Ding,[29] J. H. Do,[70] L. D'Orazio,[41] O. Drapier,[36] A. Drees,[62] K. A. Drees,[6] M. Dumancic,[68] J. M. Durham,[39] A. Durum,[25] T. Elder,[21] T. Engelmore,[14] A. Enokizono,[56,58] S. Esumi,[66] K. O. Eyser,[7] B. Fadem,[44] W. Fan,[62] N. Feege,[62] D. E. Fields,[49] M. Finger,[9] M. Finger, Jr.,[9] F. Fleuret,[36] S. L. Fokin,[34] J. E. Frantz,[51] A. Franz,[7] A. D. Frawley,[20] Y. Fukao,[32] Y. Fukuda,[66] T. Fusayasu,[46] K. Gainey,[1] C. Gal,[62] P. Garg,[3,62] A. Garishvili,[64] I. Garishvili,[38] H. Ge,[62] F. Giordano,[26] A. Glenn,[38] X. Gong,[61] M. Gonin,[36] Y. Goto,[56,57] R. Granier de Cassagnac,[36] N. Grau,[2] S. V. Greene,[67] M. Grosse Perdekamp,[26] Y. Gu,[61] T. Gunji,[12] H. Guragain,[21] T. Hachiya,[57] J. S. Haggerty,[7] K. I. Hahn,[19] H. Hamagaki,[12] S. Y. Han,[19] J. Hanks,[62] S. Hasegawa,[30] T. O. S. Haseler,[21] K. Hashimoto,[56,58] R. Hayano,[12] X. He,[21] T. K. Hemmick,[62] T. Hester,[8] J. C. Hill,[29] K. Hill,[13] R. S. Hollis,[8] K. Homma,[23] B. Hong,[33] T. Hoshino,[23] N. Hotvedt,[29] J. Huang,[7,39] S. Huang,[67] T. Ichihara,[56,57] Y. Ikeda,[56] K. Imai,[30] Y. Imazu,[56] J. Imrek,[16] M. Inaba,[66] A. Iordanova,[8] D. Isenhower,[1] A. Isinhue,[44] Y. Ito,[47] D. Ivanishchev,[55] B. V. Jacak,[62] S. J. Jeon,[45] M. Jezghani,[21] Z. Ji,[62] J. Jia,[7,61] X. Jiang,[39] B. M. Johnson,[7,21] K. S. Joo,[45] V. Jorjadze,[62] D. Jouan,[53] D. S. Jumper,[26] J. Kamin,[62] S. Kanda,[12,32] B. H. Kang,[22] J. H. Kang,[70] J. S. Kang,[22] D. Kapukchyan,[8] J. Kapustinsky,[39] S. Karthas,[62] D. Kawall,[42] A. V. Kazantsev,[34] J. A. Key,[49] V. Khachatryan,[62] P. K. Khandai,[3] A. Khanzadeev,[55] K. M. Kijima,[23] C. Kim,[8,33] D. J. Kim,[31] E.-J. Kim,[10] M. Kim,[60] M. H. Kim,[33] Y.-J. Kim,[26] Y. K. Kim,[22] D. Kincses,[17] E. Kistenev,[7] J. Klatsky,[20] D. Kleinjan,[8] P. Kline,[62] T. Koblesky,[13] M. Kofarago,[17,69] B. Komkov,[55] J. Koster,[57] D. Kotchetkov,[51] D. Kotov,[55,59] F. Krizek,[31] S. Kudo,[66] K. Kurita,[58] M. Kurosawa,[56,57] Y. Kwon,[70] R. Lacey,[61] Y. S. Lai,[14] J. G. Lajoie,[29] E. O. Lallow,[44] A. Lebedev,[29] D. M. Lee,[39] G. H. Lee,[10] J. Lee,[19,63] K. B. Lee,[39] K. S. Lee,[33] S. H. Lee,[62] M. J. Leitch,[39] M. Leitgab,[26] Y. H. Leung,[62] B. Lewis,[62] N. A. Lewis,[43] X. Li,[11] X. Li,[39] S. H. Lim,[39,70] L. D. Liu,[54] M. X. Liu,[39] V.-R. Loggins,[26] S. Lokos,[17] D. Lynch,[7] C. F. Maguire,[67] T. Majoros,[16] Y. I. Makdisi,[6] M. Makek,[68,71] M. Malaev,[55] A. Manion,[62] V. I. Manko,[34] E. Mannel,[7] H. Masuda,[58] M. McCumber,[13,39] P. L. McGaughey,[39] D. McGlinchey,[13,20] C. McKinney,[26] A. Meles,[50] M. Mendoza,[8] B. Meredith,[26] W. J. Metzger,[18] Y. Miake,[66] T. Mibe,[32] A. C. Mignerey,[41] D. E. Mihalik,[62] A. Milov,[68] D. K. Mishra,[4] J. T. Mitchell,[7] G. Mitsuka,[57] S. Miyasaka,[56,65] S. Mizuno,[56,66] A. K. Mohanty,[4] S. Mohapatra,[61] T. Moon,[70] D. P. Morrison,[7] S. I. M. Morrow,[67] M. Moskowitz,[44] T. V. Moukhanova,[34] T. Murakami,[35,56] J. Murata,[56,58] A. Mwai,[61] T. Nagae,[35] K. Nagai,[65] S. Nagamiya,[32,56] K. Nagashima,[23] T. Nagashima,[58] J. L. Nagle,[13] M. I. Nagy,[17] I. Nakagawa,[56,57] H. Nakagomi,[56,66] Y. Nakamiya,[23] K. R. Nakamura,[35,56] T. Nakamura,[56] K. Nakano,[56,65] C. Nattrass,[64] P. K. Netrakanti,[4] M. Nihashi,[23,56] T. Niida,[66] R. Nouicer,[7,57] T. Novák,[18,69] N. Novitzky,[31,62] R. Novotny,[15] A. S. Nyanin,[34] E. O'Brien,[7] C. A. Ogilvie,[29] H. Oide,[12] K. Okada,[57] J. D. Orjuela Koop,[13] J. D. Osborn,[43] A. Oskarsson,[40] K. Ozawa,[32,66] R. Pak,[7] V. Pantuev,[27] V. Papavassiliou,[50] I. H. Park,[19,63] J. S. Park,[60] S. Park,[56,60,62] S. K. Park,[33] S. F. Pate,[50] L. Patel,[21] M. Patel,[29] J.-C. Peng,[26] W. Peng,[67] D. V. Perepelitsa,[7,13,14] G. D. N. Perera,[50] D. Yu. Peressounko,[34] C. E. PerezLara,[62] J. Perry,[29] R. Petti,[7,62] M. Phipps,[7,26] C. Pinkenburg,[7] R. P. Pisani,[7] A. Pun,[51] M. L. Purschke,[7] H. Qu,[1] P. V. Radzevich,[59] J. Rak,[31] I. Ravinovich,[68] K. F. Read,[52,64] D. Reynolds,[61] V. Riabov,[48,55] Y. Riabov,[55,59] E. Richardson,[41] D. Richford,[5] T. Rinn,[29] N. Riveli,[51] D. Roach,[67] S. D. Rolnick,[8] M. Rosati,[29] Z. Rowan,[5] J. Runchey,[29] M. S. Ryu,[22] B. Sahlmueller,[62] N. Saito,[32] T. Sakaguchi,[7] H. Sako,[30] V. Samsonov,[48,55] M. Sarsour,[21] K. Sato,[66] S. Sato,[30] S. Sawada,[32] B. Schaefer,[67] B. K. Schmoll,[64] K. Sedgwick,[8] J. Seele,[57] R. Seidl,[56,57] Y. Sekiguchi,[12] A. Sen,[21,29,64] R. Seto,[8] P. Sett,[4] A. Sexton,[41] D. Sharma,[62] A. Shaver,[29] I. Shein,[25] T.-A. Shibata,[56,65] K. Shigaki,[23] M. Shimomura,[29,47] K. Shoji,[56] P. Shukla,[4] A. Sickles,[7,26] C. L. Silva,[39] D. Silvermyr,[40,52] B. K. Singh,[3] C. P. Singh,[3] V. Singh,[3] M. J. Skoby,[43] M. Skolnik,[44] M. Slunečka,[9] K. L. Smith,[20] S. Solano,[44] R. A. Soltz,[38] W. E. Sondheim,[39] S. P. Sorensen,[64] I. V. Sourikova,[7] P. W. Stankus,[52] P. Steinberg,[7] E. Stenlund,[40] M. Stepanov,[42,*] A. Ster,[69] S. P. Stoll,[7] M. R. Stone,[13] T. Sugitate,[23] A. Sukhanov,[7] J. Sun,[62] S. Syed,[21] A. Takahara,[12] A. Takeda,[47] A. Taketani,[56,57] Y. Tanaka,[46] K. Tanida,[30,57,60] M. J. Tannenbaum,[7] S. Tarafdar,[3,67,68] A. Taranenko,[48,61] G. Tarnai,[16] E. Tennant,[50] R. Tieulent,[21] A. Timilsina,[29] T. Todoroki,[56,66] M. Tomášek,[15,28] H. Torii,[12] C. L. Towell,[1] R. S. Towell,[1] I. Tserruya,[68] Y. Ueda,[23] B. Ujvari,[16] H. W. van Hecke,[39] M. Vargyas,[17,69] S. Vazquez-Carson,[13] E. Vazquez-Zambrano,[14] A. Veicht,[14] J. Velkovska,[67] R. Vértesi,[69] M. Virius,[15] V. Vrba,[15,28] E. Vznuzdaev,[55] X. R. Wang,[50,57] Z. Wang,[5] D. Watanabe,[23] K. Watanabe,[56,58] Y. Watanabe,[56,57] Y. S. Watanabe,[12,32] F. Wei,[50] S. Whitaker,[29] S. Wolin,[26] C. P. Wong,[21] C. L. Woody,[7] M. Wysocki,[52] B. Xia,[51] C. Xu,[50] Q. Xu,[67] Y. L. Yamaguchi,[12,57,62] A. Yanovich,[25] P. Yin,[13]

S. Yokkaichi,[56,57] J. H. Yoo,[33] I. Yoon,[60] Z. You,[39] I. Younus,[37,49] H. Yu,[50,54] I. E. Yushmanov,[34] W. A. Zajc,[14] A. Zelenski,[6] S. Zharko,[59] S. Zhou,[11] and L. Zou[8]

(PHENIX Collaboration)

[1]*Abilene Christian University, Abilene, Texas 79699, USA*
[2]*Department of Physics, Augustana University, Sioux Falls, South Dakota 57197, USA*
[3]*Department of Physics, Banaras Hindu University, Varanasi 221005, India*
[4]*Bhabha Atomic Research Centre, Bombay 400 085, India*
[5]*Baruch College, City University of New York, New York, New York 10010 USA*
[6]*Collider-Accelerator Department, Brookhaven National Laboratory, Upton, New York 11973-5000, USA*
[7]*Physics Department, Brookhaven National Laboratory, Upton, New York 11973-5000, USA*
[8]*University of California–Riverside, Riverside, California 92521, USA*
[9]*Charles University, Ovocný trh 5, Praha 1, 116 36 Prague, Czech Republic*
[10]*Chonbuk National University, Jeonju 561-756, Korea*
[11]*Science and Technology on Nuclear Data Laboratory, China Institute of Atomic Energy, Beijing 102413, People's Republic of China*
[12]*Center for Nuclear Study, Graduate School of Science, University of Tokyo, 7-3-1 Hongo, Bunkyo, Tokyo 113-0033, Japan*
[13]*University of Colorado, Boulder, Colorado 80309, USA*
[14]*Columbia University, New York, New York 10027 and Nevis Laboratories, Irvington, New York 10533, USA*
[15]*Czech Technical University, Zikova 4, 166 36 Prague 6, Czech Republic*
[16]*Debrecen University, H-4010 Debrecen, Egyetem tér 1, Hungary*
[17]*ELTE, Eötvös Loránd University, H-1117 Budapest, Pázmány P. s. 1/A, Hungary*
[18]*Eszterházy Károly University, Károly Róbert Campus, H-3200 Gyöngyös, Mátrai út 36, Hungary*
[19]*Ewha Womans University, Seoul 120-750, Korea*
[20]*Florida State University, Tallahassee, Florida 32306, USA*
[21]*Georgia State University, Atlanta, Georgia 30303, USA*
[22]*Hanyang University, Seoul 133-792, Korea*
[23]*Hiroshima University, Kagamiyama, Higashi-Hiroshima 739-8526, Japan*
[24]*Department of Physics and Astronomy, Howard University, Washington, DC 20059, USA*
[25]*IHEP Protvino, State Research Center of Russian Federation, Institute for High Energy Physics, Protvino 142281, Russia*
[26]*University of Illinois at Urbana-Champaign, Urbana, Illinois 61801, USA*
[27]*Institute for Nuclear Research of the Russian Academy of Sciences, prospekt 60-letiya Oktyabrya 7a, Moscow 117312, Russia*
[28]*Institute of Physics, Academy of Sciences of the Czech Republic, Na Slovance 2, 182 21 Prague 8, Czech Republic*
[29]*Iowa State University, Ames, Iowa 50011, USA*
[30]*Advanced Science Research Center, Japan Atomic Energy Agency, 2-4 Shirakata Shirane, Tokai-mura, Naka-gun, Ibaraki-ken 319-1195, Japan*
[31]*Helsinki Institute of Physics and University of Jyväskylä, P.O. Box 35, FI-40014 Jyväskylä, Finland*
[32]*KEK, High Energy Accelerator Research Organization, Tsukuba, Ibaraki 305-0801, Japan*
[33]*Korea University, Seoul 136-701, Korea*
[34]*National Research Center "Kurchatov Institute", Moscow 123098 Russia*
[35]*Kyoto University, Kyoto 606-8502, Japan*
[36]*Laboratoire Leprince-Ringuet, Ecole Polytechnique, CNRS-IN2P3, Route de Saclay, F-91128 Palaiseau, France*
[37]*Physics Department, Lahore University of Management Sciences, Lahore 54792, Pakistan*
[38]*Lawrence Livermore National Laboratory, Livermore, California 94550, USA*
[39]*Los Alamos National Laboratory, Los Alamos, New Mexico 87545, USA*
[40]*Department of Physics, Lund University, Box 118, SE-221 00 Lund, Sweden*
[41]*University of Maryland, College Park, Maryland 20742, USA*
[42]*Department of Physics, University of Massachusetts, Amherst, Massachusetts 01003-9337, USA*
[43]*Department of Physics, University of Michigan, Ann Arbor, Michigan 48109-1040, USA*
[44]*Muhlenberg College, Allentown, Pennsylvania 18104-5586, USA*
[45]*Myongji University, Yongin, Kyonggido 449-728, Korea*
[46]*Nagasaki Institute of Applied Science, Nagasaki-shi, Nagasaki 851-0193, Japan*
[47]*Nara Women's University, Kita-uoya Nishi-machi Nara 630-8506, Japan*

[48]National Research Nuclear University, MEPhI, Moscow Engineering Physics Institute, Moscow 115409, Russia
[49]University of New Mexico, Albuquerque, New Mexico 87131, USA
[50]New Mexico State University, Las Cruces, New Mexico 88003, USA
[51]Department of Physics and Astronomy, Ohio University, Athens, Ohio 45701, USA
[52]Oak Ridge National Laboratory, Oak Ridge, Tennessee 37831, USA
[53]IPN-Orsay, Université Paris-Sud, CNRS/IN2P3, Université Paris-Saclay, BP1, F-91406 Orsay, France
[54]Peking University, Beijing 100871, People's Republic of China
[55]PNPI, Petersburg Nuclear Physics Institute, Gatchina, Leningrad region 188300, Russia
[56]RIKEN Nishina Center for Accelerator-Based Science, Wako, Saitama 351-0198, Japan
[57]RIKEN BNL Research Center, Brookhaven National Laboratory, Upton, New York 11973-5000, USA
[58]Physics Department, Rikkyo University, 3-34-1 Nishi-Ikebukuro, Toshima, Tokyo 171-8501, Japan
[59]Saint Petersburg State Polytechnic University, St. Petersburg, 195251 Russia
[60]Department of Physics and Astronomy, Seoul National University, Seoul 151-742, Korea
[61]Chemistry Department, Stony Brook University, SUNY, Stony Brook, New York 11794-3400, USA
[62]Department of Physics and Astronomy, Stony Brook University, SUNY, Stony Brook, New York 11794-3800, USA
[63]Sungkyunkwan University, Suwon 440-746, Korea
[64]University of Tennessee, Knoxville, Tennessee 37996, USA
[65]Department of Physics, Tokyo Institute of Technology, Oh-okayama, Meguro, Tokyo 152-8551, Japan
[66]Center for Integrated Research in Fundamental Science and Engineering, University of Tsukuba, Tsukuba, Ibaraki 305, Japan
[67]Vanderbilt University, Nashville, Tennessee 37235, USA
[68]Weizmann Institute, Rehovot 76100, Israel
[69]Institute for Particle and Nuclear Physics, Wigner Research Centre for Physics, Hungarian Academy of Sciences (Wigner RCP, RMKI) H-1525 Budapest 114, PO Box 49, Budapest, Hungary
[70]Yonsei University, IPAP, Seoul 120-749, Korea
[71]Department of Physics, Faculty of Science, University of Zagreb, Bijenička c. 32 HR-10002 Zagreb, Croatia

(Received 29 March 2017; published 12 June 2017)

The cross section and transverse single-spin asymmetries of μ^- and μ^+ from open heavy-flavor decays in polarized $p+p$ collisions at $\sqrt{s}=200$ GeV were measured by the PHENIX experiment during 2012 at the Relativistic Heavy Ion Collider. Because heavy-flavor production is dominated by gluon-gluon interactions at $\sqrt{s}=200$ GeV, these measurements offer a unique opportunity to obtain information on the trigluon correlation functions. The measurements are performed at forward and backward rapidity ($1.4<|y|<2.0$) over the transverse momentum range of $1.25<p_T<7$ GeV/c for the cross section and $1.25<p_T<5$ GeV/c for the asymmetry measurements. The obtained cross section is compared to a fixed-order-plus-next-to-leading-log perturbative-quantum-chromodynamics calculation. The asymmetry results are consistent with zero within uncertainties, and a model calculation based on twist-3 three-gluon correlations agrees with the data.

DOI: 10.1103/PhysRevD.95.112001

I. INTRODUCTION

Transverse single-spin asymmetry (TSSA) phenomena have gained substantial attention in both experimental and theoretical studies in recent years. The existence of TSSAs has been well established in the production of light mesons at forward rapidity in transversely polarized $p+p$ collisions at energies ranging from the Zero Gradient Synchrotron up to the Relativistic Heavy Ion Collider (RHIC). Surprisingly large but oppositely signed TSSA results were first observed in π^+ and π^- production at large Feynman-x (x_F) in transversely polarized $p+p$ collisions at $\sqrt{s}=4.9$ GeV [1]. These results surprised the quantum-chromodynamics (QCD) community because they disagreed with the expectation from the naive perturbative QCD of very small spin asymmetries [2]. The large TSSA of pion production has been subsequently observed in hadronic collisions over a range of energies extending up to $\sqrt{s}=500$ GeV for π^0 ($\sqrt{s}=200$ GeV for $\pi^\pm$) [3–12]. Furthermore, TSSA in η meson production has also been studied at forward rapidity [13,14]. The results are consistent with the observed π^0 asymmetries at various energies in the overlapping x_F regions. Two theoretical

*Deceased.
†akiba@rcf.rhic.bnl.gov

formalisms within the perturbative QCD framework have been proposed to explain the origin of these large TSSAs at forward rapidity. Both formalisms connect the TSSA to the transverse motion of the partons inside the transversely polarized nucleon and/or to spin-dependent quark fragmentation.

One framework is based on the transverse-momentum-dependent (TMD) parton distribution and fragmentation functions, called TMD factorization. The initial state contributions are originating from the Sivers function [15,16], which describes the correlation between the transverse spin of the nucleon and the parton transverse momentum in the initial state. The final state contribution originates from the quark transversity distribution and the Collins [17] fragmentation function, which describes the fragmentation of a transversely polarized quark into a final state hadron with nonzero transverse momentum relative to the parton direction. This framework requires two observed scales where only one needs to be hard and both effects have been observed in SIDIS measurements [18,19]. However, TMD factorization cannot be used in the interpretation of hadron production in $p+p$ collisions as only one hard scale is available [20].

A second framework, applicable to our study, follows the QCD collinear factorization approach. The collinear, higher-twist effects become more important in generating a large TSSA when there is only one observed momentum scale that is much larger than the nonperturbative hadronic scale $\Lambda_{\rm QCD} \approx 200$ MeV [21,22]. A large TSSA can be generated from the twist-3, transverse-spin-dependent, multiparton correlation functions in the initial state or fragmentation functions in the final state.

At RHIC energies, gluon-gluon interaction processes dominate heavy quark production [23], so heavy quarks serve to isolate the gluon contribution to the asymmetries. PHENIX has measured the TSSA (A_N) of J/ψ in central and forward rapidity [24]. Theoretical predictions of the J/ψ single-spin asymmetry are complicated by the lack of good understanding of the J/ψ production mechanism [25]. In addition, there are feed-down contributions from higher resonance states in inclusive J/ψ production [26]. On the other hand, the effect of pure gluonic correlation functions on D-meson production in transversely polarized $p+p$ collisions has been extensively studied within the twist-3 mechanism in the framework of collinear factorization [27,28]. However, it is difficult to constrain the trigluon correlation functions due to the lack of experimental results. Future measurements including D-meson production are proposed at the Large Hadron Collider [29].

This paper reports on measurements of the cross section and TSSA for muons from open heavy-flavor decays in polarized $p+p$ collisions at $\sqrt{s} = 200$ GeV. Results are presented for muons from semileptonic decays of open heavy-flavor hadrons, mainly $D \to \mu + X$ and $B \to \mu + X$, in the forward and backward rapidity regions ($1.4 < |y| < 2.0$); the accessible momentum fraction of gluons in the proton is 0.0125–0.0135 and 0.08–0.14 in the backward ($x_F < 0$) and forward ($x_F > 0$) regions with respect to the polarized beam direction, respectively. Section II describes the RHIC polarized proton beams and the PHENIX experimental setup. The detailed analysis of muons from open heavy flavor, including cross sections and TSSAs, will be described in Sec. III, and the results will be presented in Sec. IV. Finally, a discussion of the results and their possible implications will be provided in Sec. V.

II. EXPERIMENTAL SETUP

A. The PHENIX experiment

The PHENIX detector comprises two central arms at midrapidity and two muon arms at forward and backward rapidity [30]. As shown in Fig. 1, two muon spectrometers cover the full azimuthal angle in the pseudorapidity range $1.2 < \eta < 2.4$ (north arm) and $-2.2 < \eta < -1.2$ (south arm). In front of each muon arm, there are about seven interaction lengths (λ_I) of copper-and-iron absorber which provides a rejection factor of 1000 for charged pions, and an additional stainless-steel absorber (2 λ_I in total) installed in 2011 contributes to further suppress the hadronic background [31,32]. Each muon arm has three stations of cathode strip chambers, muon tracker (MuTr), for momentum measurement, and five layers (labeled from Gap0 to Gap4) of proportional tube planes, muon identifier (MuID), for muon identification. Each MuID gap comprises a plane of absorber ($\sim 1\lambda_I$) and two planes of Iarrocci tubes whose orientation is along either the horizontal or the vertical direction in each plane. The MuID also provides a trigger for events containing one or more muon candidates.

The minimum bias (MB) trigger is provided by the beam-beam counters (BBC) [33], which comprise two arrays of 64 quartz Čerenkov detectors to detect charged particles at high pseudorapidity. Each detector is located at $z = \pm 144$ cm from the interaction point and covers the pseudorapidity range $3.1 < |\eta| < 3.9$. The BBC also determines the collision-vertex position ($z_{\rm vtx}$) along the beam axis, with a resolution of roughly 2 cm in $p+p$ collisions.

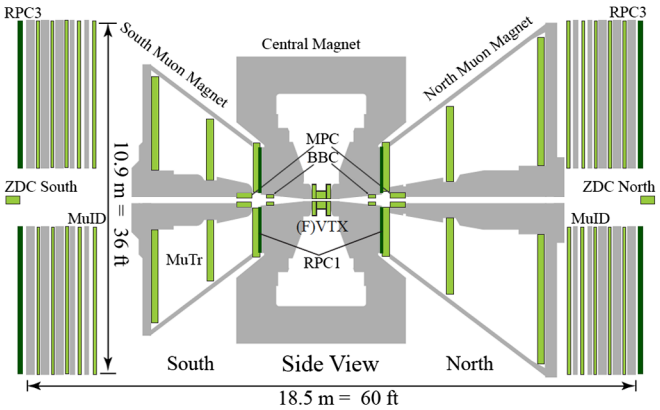

FIG. 1. Side view of the PHENIX detector in the 2012 run.

B. RHIC polarized beams

RHIC is a unique, polarized $p+p$ collider located at Brookhaven National Laboratory. RHIC comprises two countercirculating storage rings, in each of which as many as 120 polarized-proton bunches can be accelerated to a maximum energy of 255 GeV per proton.

In the 2012 run, the beam injected into RHIC typically consisted of 109 filled bunches in each ring. The bunches collided with a one-to-one correspondence with a 106 ns separation. Predefined polarization patterns for every eight bunches were changed fill by fill in order to reduce systematic effects. Two polarimeters are used to determine the beam polarizations. One is a hydrogen-jet polarimeter, which takes several hours to measure the absolute polarization [34]. The other is a fast, proton-carbon polarimeter, which measures relative changes in the magnitude of the polarization and any variations across the transverse profile of the beam several times per fill [35,36]. During the $\sqrt{s}=$ 200 GeV run in 2012, the polarization direction in the PHENIX interaction region was transverse. The average clockwise-beam (known as blue beam) polarization for the data used in this analysis was $P=0.64\pm0.03$, and the average counterclockwise-beam (yellow beam) polarization was $P=0.59\pm0.03$. There is a 3.4% global scale uncertainty in the measured A_N due to the polarization uncertainty.

III. DATA ANALYSIS

A. Data set

We analyzed a data set from transversely polarized $p+p$ collisions at $\sqrt{s}=200$ GeV collected with the PHENIX detector in 2012 with an integrated luminosity of 9.2 pb^{-1}. These data have been recorded by using the MuID trigger in coincidence with the BBC trigger. The BBC trigger requires at least one hit in both BBCs. The BBC trigger efficiency for MB $p+p$ events (events containing muons from open heavy flavor) is 55% (79%) [37] with the van der Meer scan technique [38]. The MuID trigger serves to select events containing at least one MuID track reaching Gap3 or Gap4.

B. Yield of muons from open heavy flavor

PHENIX has reported several measurements of muons from open heavy-flavor decays in various collision systems [39,40]. Similar methods developed in the previous analyses for background estimation are used in this analysis. Because of the benefit of the additional absorber material, the measurement of positively charged muons from open heavy-flavor decays is possible in PHENIX for the first time with these data.

1. Muon-candidate selection

We choose tracks penetrating through all the MuID gaps as good muon candidates from events for which the BBC z vertex is within ±25 cm. Track quality cuts, shown in Table I, are also required to reject background tracks. DG0 is the distance between the projected positions of a MuTr track and a MuID track at the z position of the MuID Gap0. DDG0 is the angular difference between the two projected positions used in the DG0. $r_{\rm ref}$ is the distance between the interaction point and a projected position of a MuID track at $z=0$. $p\cdot(\theta_{\rm MuTr}-\theta_{\rm vtx})$ is the polar scattering angle of a track inside the absorber scaled by the momentum, where $\theta_{\rm vtx}$ is the angle at the vertex and $\theta_{\rm MuTr}$ is the angle at the MuTr Station 1. Two cuts, on $p\cdot(\theta_{\rm MuTr}-\theta_{\rm vtx})$ and χ^2 at $z_{\rm vtx}$, are effective for rejecting tracks suffering from large multiple scattering or decaying to muons inside the absorber. Track quality cuts are determined with the help of a Monte Carlo simulation with GEANT4 [41]; the cut values vary with the momentum of the track.

TABLE I. Track selection cuts used in this analysis. Cut values vary with the p_T of track; those shown here are for the lowest-p_T bin ($1.25<p_T<1.5$ GeV/c).

DG0 <20 cm (South), 10 cm (North)
DDG0 <8 deg.
$r_{\rm ref}<125$ cm
Number of hits in MuTr >12, $\chi^2_{\rm MuTr}/{\rm ndf}<10$
Number of hits in MuID >6, $\chi^2_{\rm MuID}/{\rm ndf}<5$
$p\cdot(\theta_{\rm MuTr}-\theta_{\rm vtx})<0.2$ rad $\cdot$ GeV/c
χ^2 of track projection to $z_{\rm vtx}<4$

In this analysis, we also use tracks that stopped at MuID Gap3 for background estimation, although these tracks are not considered as muon candidates. After applying a proper p_z cut ($p_z\sim3.8$ GeV/c), we obtain a data sample enriched in hadrons (called stopped hadrons) [39]. These tracks are used to determine the punch-through hadron background which arises from hadrons traversing through all MuID layers without decay; this background is described in more detail in the next section.

2. Background estimation

The primary sources of background tracks are charged pions and kaons. Decay muons from $\pi^\pm$ and $K^\pm$ are the dominant background for $p_T<5$ GeV/c, while the fraction of punch-through hadrons becomes larger at $p_T>5$ GeV/c. Another background component is muons from J/ψ decays. The contribution from J/ψ decay is small in the low-p_T region but increases up to 20% of muons from inclusive heavy-flavor decays at $p_T\sim5$ GeV/c. Backgrounds from light resonances (ϕ, ρ, and ω) or other quarkonium states (χ_c, ψ', and Υ) are negligible [39,42]. Therefore, the number of muons from open heavy-flavor decays is obtained as

$$N_{\rm HF}=N_{\rm incl}/\varepsilon_{\rm trig}-N_{\rm DM}-N_{\rm PH}-N_{J/\psi\to\mu}, \qquad (1)$$

where $N_{\rm HF}$ is the number of muons from open heavy-flavor decays, $N_{\rm incl}$ is the number of muon candidates passing

through all track quality cuts in Table I, $\varepsilon_{\rm trig}$ is the trigger efficiency of the MuID trigger, $N_{\rm DM}$ is the estimated number of decay muons from $\pi^{\pm}$ and $K^{\pm}$, $N_{\rm PH}$ is the estimated number of punch-through hadrons, and $N_{J/\psi\to\mu}$ is the estimated number of muons from J/ψ decay. The trigger efficiency correction should be taken into account before subtracting the background, because the simulation of the backgrounds does not include any inefficiency of the MuID trigger. The MuID trigger efficiency is evaluated with data by measuring the fraction of MUID triggers in non-MUID triggered events containing tracks at MuID Gap3 or Gap4.

To estimate the hadronic background ($N_{\rm DM}$ and $N_{\rm PH}$), the hadron-cocktail method, developed for the previous analysis [39,42], is used. Initial particle distributions for the hadron-cocktail simulation are estimated from measurements of charged pions and kaons at midrapidity [43,44]. The PYTHIA event generator [45] is used to extrapolate the p_T spectra at midrapidity to the forward rapidity region. To obtain enough statistics of reconstructed tracks in the high-p_T region, a p_T^3 weight is applied to the estimated p_T spectra for the simulation and the simulation output is reweighted by $1/p_T^3$ for a proper comparison with the data. Based on these initial hadron distributions, a full chain of detector simulation with GEANT4 [41] and track reconstruction is performed. Because of uncertainties in the estimation of input distributions and hadron-shower simulation with the thick absorber in front of the MuTr, an additional, data-driven, tuning procedure of the simulation is needed to determine the background more precisely. Two methods, described below, are used to tune the hadron-cocktail simulation:

Normalized $z_{\rm vtx}$ distribution: The $z_{\rm vtx}$ distribution of tracks ($dN_\mu/dz_{\rm vtx}$) normalized by the $z_{\rm vtx}$ distribution of MB events ($dN_{\rm evt}/dz_{\rm vtx}$) provides a good constraint on the decay muon background. Because the distance from $z_{\rm vtx}$ to the front absorber is relatively short compared to the decay length of $\pi^{\pm}$ and $K^{\pm}$, the production of decay muons shows a linear dependence on $z_{\rm vtx}$. Therefore, the number of decay muons can be estimated by matching the slope in the normalized $z_{\rm vtx}$ distribution at MuID Gap4 for each p_T bin. More details are described in [39].

Stopped hadrons: Hadrons stopping at MuID Gap3 can be removed with an appropriate momentum cut ($p_z \sim 3.8$ GeV/c) as described in the previous section. The remaining stopped muons are less than 10% in the tracks at MuID Gap3, based on the simulation study. The punch-through hadron background at the last MuID gap can be estimated by matching the p_T distribution of stopped hadrons at MuID Gap3.

After tuning the hadron-cocktail simulation, the decay muons ($N_{\rm DM}$) from the normalized $z_{\rm vtx}$ distribution matching and the punch-through hadrons ($N_{\rm PH}$) from the stopped-hadron matching are combined for the final estimate of the background from light hadrons. For the decay muons at $p_T > 3$ GeV/c and the punch-through hadrons, the difference between the two methods of tuning is assigned as the systematic uncertainty. More details on the hadron-cocktail simulation and the tuning procedure are given in [39].

Muons from J/ψ decays are also subtracted in order to obtain the number of muons from open heavy-flavor decays. From the measurement of the J/ψ invariant cross section in the forward region [26] and a decay simulation, the number of muons from J/ψ decay ($N_{J/\psi\to\mu}$) can be estimated [42]. The contribution of muons from J/ψ to the muons from inclusive heavy-flavor decays is ~2% at low p_T and increases up to ~20% at $p_T > 5$ GeV/c. Because there is a $B \to J/\psi$ contribution in the inclusive J/ψ measurement, a fraction of B is included in $N_{J/\psi\to\mu}$ and subtracted as background. However, the fraction, $N_{B\to J/\psi\to\mu}/N_{\rm HF}$, is quite small based on the measurements of the $B \to J/\psi$ fraction [46].

Figure 2 shows the p_T spectra of inclusive muon tracks and estimated background components; the relative contribution from each source varies with p_T. After subtraction of backgrounds from light hadrons and J/ψ, the p_T spectra of muons from open heavy-flavor decays can be obtained. Figure 3 shows the signal-to-background ratio ($\frac{N_{\rm HF}}{N_{\rm DM}+N_{\rm PH}+N_{J/\psi\to\mu}}$) of negatively (top panel) and positively (bottom panel) charged tracks; blue open circle (red closed rectangle) points represent the results in the South (North) arm. Vertical bars (boxes) around the data points are statistical (systematic) uncertainties; details on systematic uncertainties will be described in the following section. Because K^+ has a longer nuclear interaction length than other light hadrons, the signal-to-background ratio of positively charged tracks is smaller than that of negatively charged tracks.

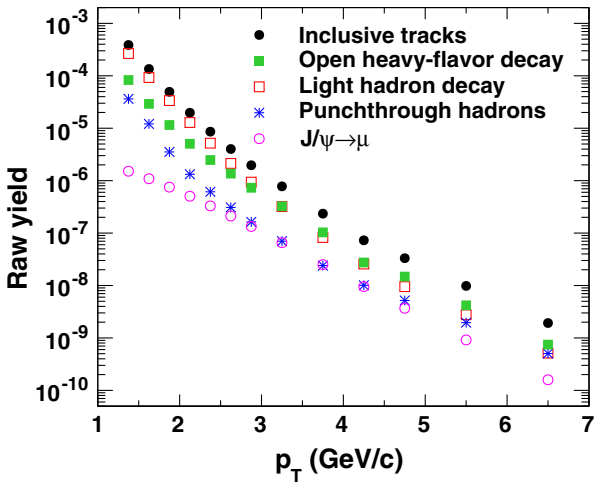

FIG. 2. p_T spectra of inclusive muon candidates and background sources from the hadron-cocktail simulation after p_T -dependent tuning.

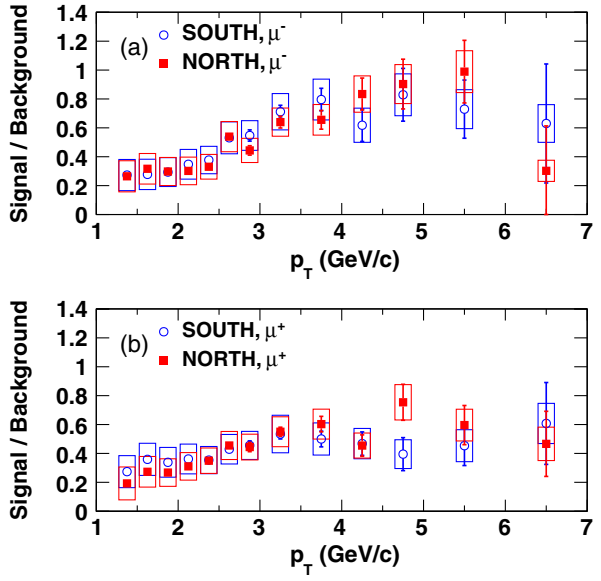

FIG. 3. Signal-to-background ratio of (a) negatively charged and (b) positively charged tracks. Each panel includes results in the North [closed (red) rectangle] and South [open (blue) circle] arms. Vertical bars (boxes) correspond to the statistical (systematic) uncertainties.

3. Acceptance and efficiency correction

The acceptance and efficiency correction is evaluated by using a single-muon simulation. The same simulation procedure as for the hadron-cocktail simulation is used, and reconstructed muons are filtered with the same track quality cuts and fiducial cuts as was applied to the data. Because detector performance throughout the data-taking period is stable, one reference run is used to calculate the correction factors. The variation of the number of muon candidates per event throughout the data-taking period is 8.1% (4.6%) for the South (North) arm, and the quadratic sum with the systematic uncertainty on the MuTr (4%) and MuID (2%) is assigned to the systematic uncertainty on the acceptance and efficiency correction.

4. Systematic uncertainty

There are three major sources of systematic uncertainty: the background estimation ($\delta_{\rm bkg}$), the acceptance and efficiency correction ($\delta_{A\varepsilon}$), and the BBC efficiency ($\delta_{\rm BBC}$).

The sources of $\delta_{\rm bkg}$ are listed here:

$\delta_{\rm trig}$ A 5% (15%) systematic uncertainty is assigned to the MuID trigger efficiency for tracks at MuID Gap4 (Gap3) by considering the statistical uncertainty of tracks in the non-MuID triggered events, and the uncertainty is included in the systematic uncertainty on the $N_{\rm DM}$ (Gap4) and $N_{\rm PH}$ (Gap3).

$\delta_{\rm sim}$ The hadron-cocktail simulation with the thick absorber ($\sim 13\lambda_I$) can be a source of systematic uncertainty. In case of the $N_{\rm DM}$ in $p_T < 3$ GeV/c where background can be constrained with muons, a 10% systematic uncertainty is assigned conservatively due to extraction of the slope in the normalized $z_{\rm vtx}$ distributions. The difference between the two methods of tuning described in Sec. III B 2 is assigned to the systematic uncertainty on the $N_{\rm DM}$ in $p_T > 3$ GeV/c and the $N_{\rm PH}$. The systematic uncertainty on the $N_{\rm DM}$ ($N_{\rm PH}$) is 10%–15% (10%–40%) depending on p_T.

$\delta_{\rm input}$ Because there is no precise measurement of $\pi^{\pm}$ and $K^{\pm}$ production at forward rapidity, a 30% systematic uncertainty is assigned to the estimation of the K/π ratio based on the systematic uncertainty of measurements at midrapidity [43,44]. The impact on $N_{\rm HF}$ is evaluated by performing the hadron-cocktail tuning procedure with various initial K/π ratios, and the variation of $N_{\rm HF}$ is less than 10%. The uncertainty on the shape of the p_T distribution is negligible, because the tuning of the hadron-cocktail simulation can take into account a p_T dependence. A 10% systematic uncertainty is assigned to $N_{\rm HF}$ conservatively.

$\delta_{J/\psi\to\mu}$ The upper and lower limit of systematic uncertainty on the J/ψ cross section measurement is taken into account for the systematic uncertainty on $N_{J/\psi\to\mu}$. The contribution from B decays is also considered. A 3% systematic uncertainty is assigned to the $N_{\rm HF}$ due to the uncertainty on the $N_{J/\psi\to\mu}$.

For the systematic uncertainty on the $N_{\rm HF}$, the $\delta_{\rm trig}$ and $\delta_{\rm sim}$ on the $N_{\rm DM}$ ($N_{\rm PH}$) are propagated into the $N_{\rm HF}$ with the ratio of $N_{\rm DM}/N_{\rm HF}$ ($N_{\rm PH}/N_{\rm HF}$). This propagated uncertainty is combined with the $\delta_{\rm input}$ and $\delta_{J/\psi\to\mu}$ on the $N_{\rm HF}$ as a quadratic sum. The $\delta_{\rm bkg}$ is 8%–40%, depending on p_T.

There are also systematic uncertainties on the acceptance and efficiency correction ($\delta_{A\varepsilon}$) and the BBC efficiency ($\delta_{\rm BBC}$); see the discussion in [37]. For the $\delta_{A\varepsilon}$, all sources described in Sec. III B 3 are added in quadrature, and 9.3% and 6.4% systematic uncertainties are assigned to the South and North arms, respectively.

Table II summarizes the systematic uncertainty on the cross section of muons from open heavy-flavor decays, and the quadratic sum of the three components is the final systematic uncertainty.

C. Transverse single-spin asymmetry

1. Determination of the TSSA

Both of the proton beams are transversely polarized at the interaction point. The TSSA (A_N) in the yield of muons from heavy-flavor decays is obtained for each beam

TABLE II. Summary of systematic uncertainties on the cross section of muons from open heavy-flavor decays.

	Component	Value
$\delta_{\rm bkg}$	Background estimation	8%–40%, varies with p_T
$\delta_{A\varepsilon}$	Acceptance and efficiency	9.3%(S), 6.4%(N)
$\delta_{\rm BBC}$	BBC efficiency	10.1%
	Sum	17%–43%, varies with p_T

separately by summing over the spin information of the other beam. The final asymmetry is calculated as the weighted average of the asymmetries for the two beams.

The maximum likelihood method is used for this measurement. The likelihood $\mathcal{L}$ is defined as

$$\mathcal{L} = \prod (1 + P \cdot A_N \sin(\phi_{\rm pol} - \phi_i)), \tag{2}$$

where P is the polarization, $\phi_{\rm pol}$ is the direction of beam polarization ($+\frac{\pi}{2}$ or $-\frac{\pi}{2}$), and ϕ_i is the azimuthal angle of each track in the PHENIX lab frame. The unbinned likelihood method is used in this study, so that the result is not biased by low statistics bins. The likelihood function is usually written in logarithmic form

$$\log \mathcal{L} = \sum \log(1 + P \cdot A_N \sin(\phi_{\rm pol} - \phi_i)). \tag{3}$$

The A_N value is determined by maximizing $\log \mathcal{L}$. The statistical uncertainty of the log-likelihood estimator is related to its second derivative,

$$\sigma^2(A_N) = \left(-\frac{\partial^2 \mathcal{L}}{\partial A_N^2} \right)^{-1}. \tag{4}$$

2. Inclusive- and background-asymmetry estimation

We study tracks that penetrate to the last MuID gap (Gap4); these tracks are created by muons from open heavy-flavor decays, punch-through hadrons, muons from light hadrons, and muons from J/ψ decay. The contribution from other sources is negligible as discussed in Sec. III B 2. To obtain the asymmetry of muons from open heavy-flavor decays ($A_N^{\rm HF}$), the asymmetry of the background from light hadrons ($A_N^{\rm h}$) and muons from J/ψ ($A_N^{J/\psi \to \mu}$) should be eliminated from the asymmetry of inclusive muon candidates ($A_N^{\rm incl}$). Because hadron tracks can be selected with the p_z cut, $A_N^{\rm h}$ is obtained from the asymmetry of stopped hadrons at MuID Gap3. Possible differences between the A_N of stopped hadrons at MuID Gap3 and the mixture of decay muons and punch-through hadrons at MuID Gap4 is studied with the hadron-cocktail simulation. The details are described in Sec. III C 3.

For the estimation of $A_N^{J/\psi \to \mu}$, a previous PHENIX $A_N^{J/\psi}$ measurement [24] is used. The asymmetry of single muons from J/ψ decay ($A_N^{J/\psi \to \mu}$) is estimated from a decay simulation with the initial $A_N^{J/\psi}$ in [24] ($A_N^{J/\psi} = -0.002 \pm 0.026$ at $x_F < 0$, and -0.026 ± 0.026 at $x_F > 0$). The initial p_T and rapidity distributions of J/ψ are taken from [26]. The obtained $A_N^{J/\psi \to \mu}$ is $-0.002^{+0.018}_{-0.022}$ at $x_F < 0$ and $-0.019^{+0.019}_{-0.025}$ at $x_F > 0$. A possible effect from J/ψ polarization is tested by assuming maximum polarization, and the variation of $A_N^{J/\psi \to \mu}$ is < 0.001. Because the variation due to J/ψ polarization is much smaller than the variation from the uncertainty of $A_N^{J/\psi}$, the J/ψ polarization effect is not included to evaluate $A_N^{J/\psi \to \mu}$ and the systematic uncertainty.

Once $A_N^{\rm h}$ and $A_N^{J/\psi \to \mu}$ are determined, the A_N of muons from open heavy-flavor decays and its uncertainty can be obtained as

$$A_N^{\rm HF} = \frac{A_N^{\rm incl} - f_{\rm h} \cdot A_N^{\rm h} - f_{J/\psi} \cdot A_N^{J/\psi \to \mu}}{1 - f_{\rm h} - f_{J/\psi}}, \tag{5}$$

$$\delta A_N^{\rm HF} = \frac{\sqrt{(\delta A_N^{\rm incl})^2 + f_{\rm h}^2 \cdot (\delta A_N^{\rm h})^2 + f_{J/\psi}^2 \cdot (\delta A_N^{J/\psi \to \mu})^2}}{1 - f_{\rm h} - f_{J/\psi}}, \tag{6}$$

where $f_{\rm h} = (N_{\rm DM} + N_{\rm PH})/N_{\rm incl}$ is the fraction of the light-hadron background, and $f_{J/\psi} = N_{J/\psi \to \mu}/N_{\rm incl}$ is the fraction of muons from J/ψ. Both fractions ($f_{\rm h}$ and $f_{J/\psi}$) are determined from the background estimation described above. $\delta A_N^{J/\psi \to \mu}$, estimated from the previous PHENIX measurement, is included in the systematic uncertainty.

3. Systematic uncertainty

The systematic uncertainty is determined from variation of $A_N^{\rm HF}$ between the upper and lower limits of each background source. An additional systematic uncertainty is derived from the comparison between the two $A_N^{\rm HF}$ calculation methods; the maximum likelihood method [Eq. (3)] and the polarization formula [Eq. (7)]. The final systematic uncertainty is calculated as the quadratic sum of systematic uncertainties from each source ($\delta A_N^{\delta f_{\rm h}}$, $\delta A_N^{\rm h}$, $\delta A_N^{J/\psi \to \mu}$, and $\delta A_N^{\rm method}$), described here:

$\delta A_N^{\delta f_{\rm h}}$ Systematic uncertainty on the fraction of light-hadron background ($\delta f_{\rm h}$) from Fig. 3 is an important source of systematic uncertainty on $A_N^{\rm HF}$. The upper and lower limits of $A_N^{\rm HF}$ are calculated using Eq. (5) with the upper and lower limits of the fraction of the light-hadron background ($f_{\rm h} \pm \delta f_{\rm h}$).

$\delta A_N^{\rm h}$ The asymmetry of the light-hadron background ($A_N^{\rm h}$) at MuID Gap4 is estimated by using stopped hadrons at MuID Gap3. Because of decay kinematics, the $A_N^{\rm h}$ at MuID Gap4 can be different from the $A_N^{\rm h}$ measured at MuID Gap3. In order to quantify the difference, a simulation study using the decay kinematics of light hadrons from the hadron cocktail in Sec. III B 2 and an input asymmetry ($A_N^{\rm input}$) is performed. $A_N^{\rm input}$ is taken as $0.02 \times p_T$ (with p_T in GeV/c) at $p_T < 5$ GeV/c and 0.1 at $p_T > 5$ GeV/c, based on the most extreme case of $A_N^{\rm h}$ measured at MuID Gap3. The detailed procedure is as follows:

(1) Generate a random spin direction ($\uparrow, \downarrow$) for all tracks.
(2) Apply a weight ($1 \pm A_N^{\rm input} \cdot \cos\phi_0$) for each track based on the manually assigned initial asymmetry ($A_N^{\rm input}$). The sign is determined from the random

polarization direction in step 1, and ϕ_0 is the azimuthal angle of the track at the generation level.

(3) Extract $A_N^{\rm reco}$ of the tracks at MuID Gap3 and Gap4 with the azimuthal angle and momentum of the reconstructed tracks by fitting the asymmetry of the two polarization cases with $A_N^{\rm reco} \cdot \cos\phi_0$.

The largest difference between $A_N^{\rm reco}$ at MuID Gap3 and Gap4 is ~0.008 in the entire p_T range, so ± 0.008 is assigned to the systematic uncertainty. In the case of x_F binning, the difference of $A_N^{\rm reco}$ at MuID Gap3 and Gap4 is quite small (<0.001).

$\delta A_N^{J/\psi\to\mu}$ The systematic uncertainty from $A_N^{J/\psi\to\mu}$ is determined from the $J/\psi \to \mu$ simulation with the upper and lower limits of $A_N^{J/\psi}$ in [24]. Propagation to $A_N^{\rm HF}$ is calculated using Eq. (5). The effect from $B \to J/\psi$ is negligible due to its small fraction in the inclusive J/ψ.

$\delta A_N^{\rm method}$ The $A_N^{\rm incl}$ results from the maximum likelihood method at Eq. (3) are compared with results using the polarization formula at Eq. (7). Because the measurement of $A_N^{\rm h}$ using tracks at MuID Gap3 suffer from large statistical fluctuations, the difference of two methods with inclusive tracks at MuID Gap4 is used for both $A_N^{\rm incl}$ and $A_N^{\rm h}$ variations using Eq. (5). $A_N(\phi)$ of inclusive tracks for each p_T or x_F bin is calculated as

$$A_N(\phi) = \frac{\sigma^{\uparrow}(\phi) - \sigma^{\downarrow}(\phi)}{\sigma^{\uparrow}(\phi) + \sigma^{\downarrow}(\phi)} = \frac{1}{P} \cdot \frac{N^{\uparrow}(\phi) - R \cdot N^{\downarrow}(\phi)}{N^{\uparrow}(\phi) + R \cdot N^{\downarrow}(\phi)}, \quad (7)$$

where P is the average beam polarization, $\sigma^{\uparrow}$ and $\sigma^{\downarrow}$ are cross sections for each polarization, $N^{\uparrow}$ and $N^{\downarrow}$ are yields for two polarizations, and $R = L^{\uparrow}/L^{\downarrow}$ is the relative luminosity where the luminosity $(L^{\uparrow}, L^{\downarrow})$ is measured by the BBC detectors. $A_N^{\rm incl}$ is calculated by fitting the $A_N(\phi)$ distribution with a function $\pm A_N \cdot \cos\phi$, where $\pm$ depends on the beam direction. The systematic uncertainty on $A_N^{\rm HF}$ is evaluated by propagating variations of $A_N^{\rm incl}$ and $A_N^{\rm h}$ between the maximum likelihood method and the polarization formula.

IV. RESULTS

A. Cross section of muons from open heavy-flavor decays

The invariant cross section of muons from open heavy-flavor decays is calculated as

$$E\frac{d^3\sigma}{dp^3} = \frac{1}{2\pi p_T \Delta p_T \Delta y} \frac{(N_{\rm HF}/\varepsilon_{\rm BBC}^{\rm HF}) \cdot \sigma_{pp}^{\rm inel}}{(N_{\rm evt}/\varepsilon_{\rm BBC}^{\rm MB}) \cdot A\varepsilon}, \quad (8)$$

where Δp_T and Δy are the bin widths in p_T and y, $N_{\rm evt}$ is the number of sampled MB events, $\varepsilon_{\rm BBC}^{\rm MB}$ ($\varepsilon_{\rm BBC}^{\rm HF}$) is the BBC correction factor for the trigger efficiency of MB events (events containing muons from open heavy-flavor decays), $A\varepsilon$ is the detector acceptance and track reconstruction efficiency, and $\sigma_{pp}^{\rm inel} = 42 \pm 3$ mb is the inelastic cross section of $p + p$ collisions at $\sqrt{s} = 200$ GeV.

Figure 4 shows the invariant cross section of positively (open square) and negatively charged (open circle) muons from open heavy-flavor decays as a function of p_T in $p + p$ collisions at $\sqrt{s} = 200$ GeV. Vertical bars (boxes) correspond to the statistical (systematic) uncertainties. The previous PHENIX results for negatively charged muons [40] are shown, and vertical bars represent total uncertainties. The bottom panel shows the ratio between positively and negatively charged muons from open heavy-flavor decays (red open circles); the two p_T spectra are consistent within the systematic uncertainties which are dominated by the uncertainty from the hadron contamination. The comparison with the previous PHENIX results for negative muons is also presented as a ratio (black diamonds); the fit function in [40] is used to make a ratio at $p_T > 4.0$ GeV/c. The uncertainties from the new results are included in the ratio, and two results are in good agreement.

B. Transverse single-spin asymmetry

The TSSA of muons from open heavy-flavor decays is calculated by using Eq. (5), and the statistical uncertainty is determined by using Eq. (6). Figures 5 and 6 present the TSSA of negatively ($A_N^{\mu^-}$) and positively ($A_N^{\mu^+}$) charged muons from open heavy flavor as a function of p_T in the forward ($x_F > 0$) and backward ($x_F < 0$) regions with respect to the polarized-proton beam direction. Figure 7 shows the TSSA versus x_F of muons from open heavy-flavor

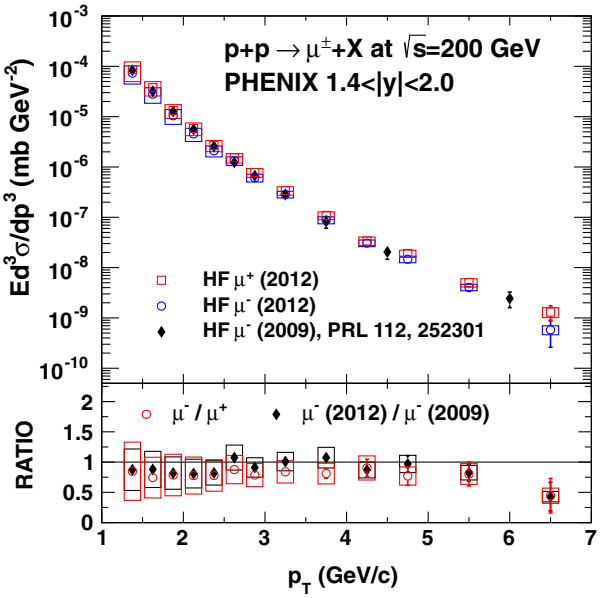

FIG. 4. (top) Invariant cross section of muons from open heavy-flavor decays as a function of p_T in $p + p$ collisions at $\sqrt{s} = 200$ GeV at forward rapidity. (bottom) Ratio of invariant cross sections. Vertical bars (boxes) correspond to the statistical (systematic) uncertainties.

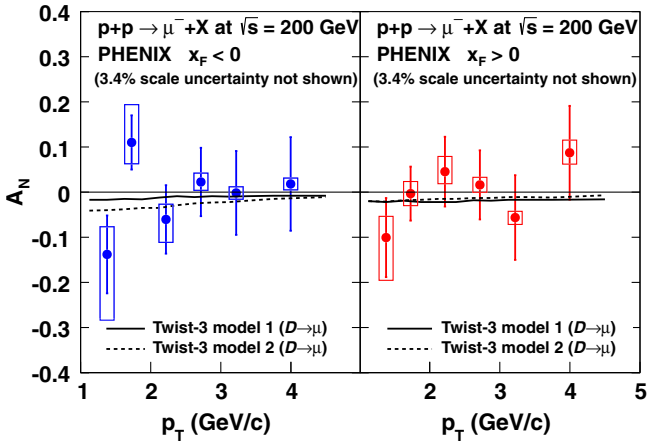

FIG. 5. A_N of negatively charged muons from open heavy-flavor decays as a function of p_T in the backward ($x_F < 0$, left) and forward ($x_F > 0$, right) regions. Vertical bars (boxes) represent statistical (systematic) uncertainties. Solid and dashed lines represent twist-3 model calculations [27], described in Sec. V.

decays. Vertical bars (boxes) represent statistical (systematic) uncertainties; a scale uncertainty from the polarization (3.4%) is not included. $A_N^{\mu^+}$ in the negative x_F region, shown in the left panel of Fig. 6, shows some indication of a negative asymmetry; in the combined p_T range of $2.5 < p_T < 5.0$ GeV/c the asymmetry is $-0.117 \pm 0.048(\text{stat}) \pm 0.037(\text{syst})$. However, the combined asymmetries for all p_T or x_F bins are consistent with zero within total uncertainties. Other results for $A_N^{\mu^+}$ at positive x_F and $A_N^{\mu^-}$ in all kinematic regions are consistent with zero within statistical uncertainties. The asymmetry results are tabulated in Tables III and IV, while Tables V and VI list the systematic uncertainties from each source. Table VII gives the invariant cross section of muons from open heavy-flavor decays vs p_T.

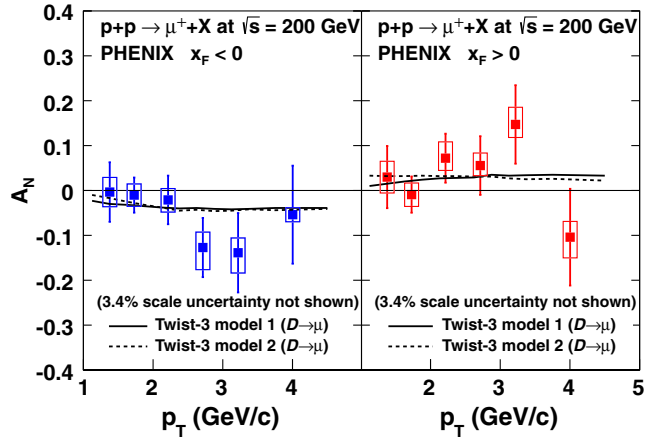

FIG. 6. A_N of positively charged muons from open heavy-flavor decays as a function of p_T in the backward ($x_F < 0$, left) and forward ($x_F > 0$, right) regions. Vertical bars (boxes) represent statistical (systematic) uncertainties. Solid and dashed lines represent twist-3 model calculations [27], described in Sec. V.

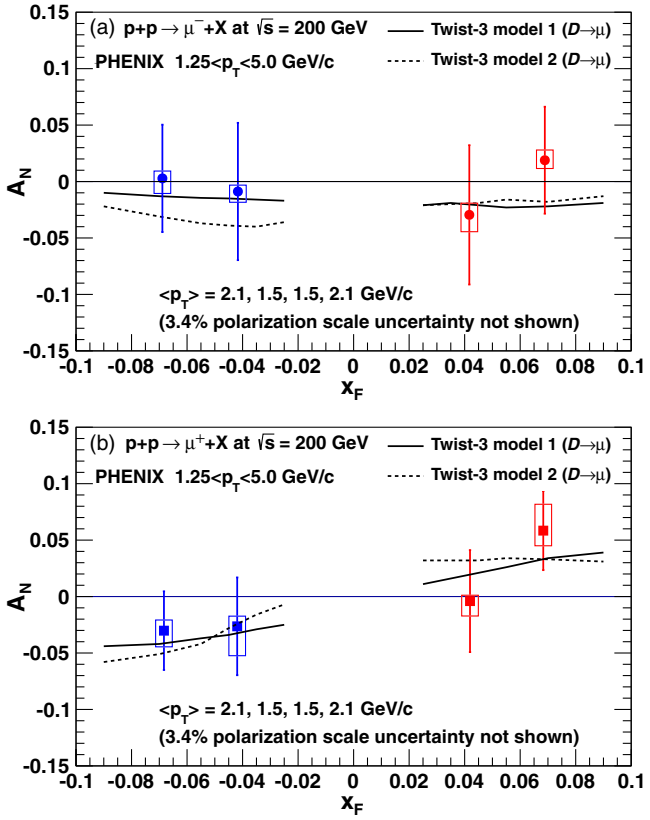

FIG. 7. A_N of (a) negatively charged and (b) positively charged muons from open heavy-flavor decays as a function of x_F, where $x_F > 0$ is along the direction of the polarized proton. Vertical bars (boxes) represent statistical (systematic) uncertainties. Solid and dashed lines represent twist-3 model calculations [27], described in Sec. V.

V. DISCUSSION

Table VII and Fig. 8 show the charge-combined, invariant cross section of muons from open heavy-flavor decays as a function of p_T. Vertical bars (boxes) in Fig. 8 correspond to the statistical (systematic) uncertainties. The solid line in Fig. 8 represents the fixed-order-plus-next-to-leading-log (FONLL) calculation of muons from open heavy-flavor decays from charm and bottom [47], and the band around the line represents the systematic uncertainty from the renormalization scale, factorization scale, and heavy (c and b) quark masses. The bottom panel shows the ratio between the data and the FONLL calculation. In general, the agreement between the data and the FONLL prediction becomes better with increasing p_T where the systematic uncertainties of both are decreasing. At $p_T < 4$ GeV/c where the charm contribution is larger than that from bottom, the measured yield is larger than the FONLL calculation, but systematic uncertainties are large in both the data and the theoretical calculation. Recently, a theoretical approach within the gluon saturation (color-glass-condensate) framework also presents the cross section of leptons from heavy-flavor decays in $p + p$ and $p + A$ collisions [48].

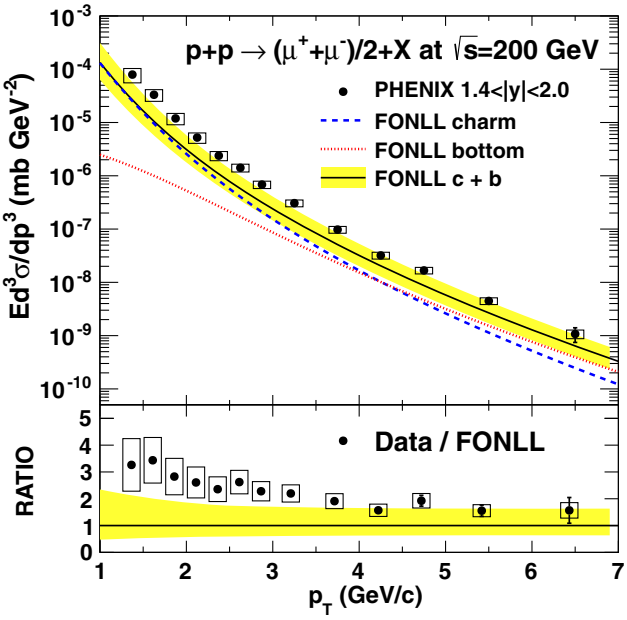

FIG. 8. (Top) Charge-combined, invariant cross section of muons from open heavy-flavor decays as a function of p_T in $p+p$ collisions at $\sqrt{s} = 200$ GeV at forward rapidity. The solid line and band represent the FONLL calculation for charm and bottom and its systematic uncertainty. The dashed and dotted curves show contributions from charm and bottom separately. (Bottom) Ratio between the data and the FONLL calculation. Vertical lines (boxes) represent statistical (systematic) uncertainties of the data.

A recent theoretical calculation [27] incorporating the collinear factorization framework makes predictions for A_N in the production of D mesons (A_N^D) produced by the gluon-fusion ($gg \to c\bar{c}$) process and therefore is sensitive to the trigluon correlation functions which depend on the momentum fraction of the gluon in the proton in the infinite-momentum frame (x-Bjorken). Two model calculations, assuming either a linear x dependence (Model 1 in Figs. 5, 6, and 7) or a $\sqrt{x}$ dependence (Model 2 in Figs. 5, 6, and 7), for the nonperturbative functions participating in the twist-3 cross section for A_N^D are introduced to compare their behavior in the small-x region, and the overall A_N^D scale is determined by assuming $|A_N^D| \leq 0.05$ at $|x_F| < 0.1$.

To compare with our results for A_N^μ, the decay kinematics and cross section of $D \to \mu$ from PYTHIA [49] have been used to convert A_N^D into A_N^μ. The theory calculations of the x_F and p_T dependence of A_N for D^0, $\bar{D}^0$, D^+, and D^- at $-0.6 < x_F^D < 0.6$ and $1 < p_T^D < 10$ GeV/c are used as the input A_N^D to the simulation. A similar procedure to that described in the systematic-uncertainty evaluation for $\delta A_N^{\rm h}$ is used. A weight of $(1 \pm A_N^D(p_T^D, x_F^D) \cdot \sin(\phi^D - \phi_{\rm pol}))$ is applied for each muon from a D meson, and the sign is determined with a random polarization direction $(\uparrow, \downarrow)$. Then, A_N^μ is extracted by fitting the asymmetry of the two polarization cases with $A_N^\mu \cdot \cos\phi^\mu$.

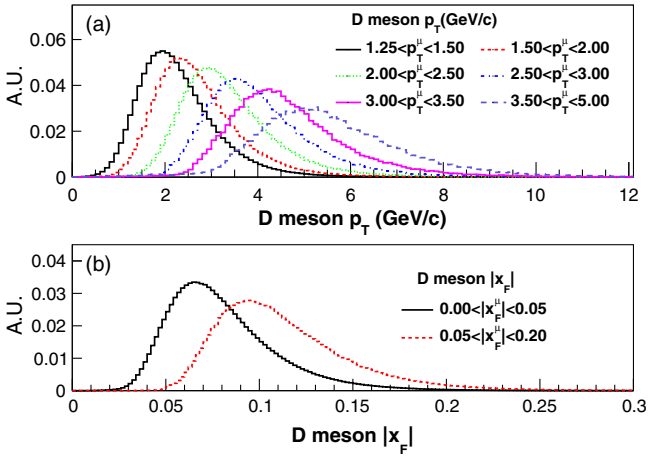

FIG. 9. (a) p_T and (b) $|x_F|$ distributions of D mesons (D^0, $\bar{D}^0$, D^+, and D^-) decaying into $\mu^\pm$ in $1.25 < p_T^\mu < 5.0$, $0.0 < |x_F^\mu| < 0.2$, and $1.4 < |y^\mu| < 2.0$ from PYTHIA. Each distribution is normalized to unity.

Figure 9 shows the p_T and $|x_F|$ distributions of D mesons which decay into muons in the kinematic range of this measurement ($1.25 < p_T^\mu < 5.0$ GeV/c, $0.0 < |x_F^\mu| < 0.2$, and $1.4 < |y^\mu| < 2.0$); accepted charm hadrons comprise D^0(18.7%), $\bar{D}^0$(20.3%), D^+(24.2%), D^-(26.1%), and others (D_s^+, D_s^-, and baryons). Because $A_N^{D^0}$ and $A_N^{D^+}$ ($A_N^{\bar{D}^0}$ and $A_N^{D^-}$) are very close in both models, the effect of potential different abundance of D mesons between the data and PYTHIA is negligible. In addition, the modification of A_N due to azimuthal smearing from the D decay is quite small (<5% relative difference between A_N^D and A_N^μ) in $p_T^\mu > 1.25$ GeV/c. One notes that muons from charm and bottom are combined in the data, and the contribution from bottom is about 2% (55%) at $p_T = 1$ GeV/c (5 GeV/c) according to the FONLL calculation shown in Fig. 8. Therefore, the charm contribution is expected to be dominant except for the last p_T bin of A_N^μ ($3.5 < p_T < 5$ GeV/c). In addition, subprocesses other than gluon fusion can contribute to the measured yield of muons from heavy-flavor decays. The converted A_N of muons from D mesons are shown in Figs. 5, 6, and 7, and both calculations are in agreement with the data within the statistical uncertainties. The difference between two models becomes larger at increasing $|x_F|$, but it is hard to distinguish these two models due to the limited x_F coverage for this measurement ($\langle|x_F^\mu|\rangle = 0.04, 0.07$).

VI. SUMMARY

We have reported the cross section and transverse single-spin asymmetry of muons from open heavy-flavor decays at $1.4 < |y| < 2.0$ in transversely polarized $p+p$ collisions at $\sqrt{s} = 200$ GeV. Comparing with previous measurements by PHENIX, the cross section and asymmetry for positively charged muons from open heavy-flavor

decays are measured for the first time with the help of additional absorber material in the PHENIX muon arms. In the comparison with the FONLL calculation, the FONLL prediction is smaller than the measured cross section at low p_T where both experimental and theoretical systematic uncertainties are large, but it shows an agreement at $p_T > 4$ GeV/c within systematic uncertainties.

Following the cross section results, we have measured the single-spin asymmetry of muons from open heavy-flavor decays for the first time. There is no clear indication of a nonzero asymmetry in the results, which have relatively large statistical uncertainties. Theoretical calculations of A_N for D-meson production which take into account trigluon correlations are converted into A_N for muons with the help of PYTHIA to compare directly with the data. The calculations are in agreement with the data within experimental uncertainties. Future studies with improved statistics (6.5 times current integrated luminosity of this analysis), using data taken with the PHENIX detector at RHIC in 2015, could provide further constraints on the trigluon correlation functions.

ACKNOWLEDGMENTS

We thank the staff of the Collider-Accelerator and Physics Departments at Brookhaven National Laboratory and the staff of the other PHENIX participating institutions for their vital contributions. We also thank S. Yoshida and Y. Koike for the theory calculation. We acknowledge support from the Office of Nuclear Physics in the Office of Science of the Department of Energy, the National Science Foundation, Abilene Christian University Research Council, Research Foundation of SUNY, and Dean of the College of Arts and Sciences, Vanderbilt University (USA), Ministry of Education, Culture, Sports, Science, and Technology and the Japan Society for the Promotion of Science (Japan), Conselho Nacional de Desenvolvimento Científico e Tecnológico and Fundação de Amparo à Pesquisa do Estado de São Paulo (Brazil), Natural Science Foundation of China (People's Republic of China), Croatian Science Foundation and Ministry of Science and Education (Croatia), Ministry of Education, Youth, and Sports (Czech Republic), Centre National de la Recherche Scientifique, Commissariat à l'Énergie Atomique, and Institut National de Physique Nucléaire et de Physique des Particules (France), Bundesministerium für Bildung und Forschung, Deutscher Akademischer Austausch Dienst, and Alexander von Humboldt Stiftung (Germany), National Science Fund, OTKA, EFOP, and the Ch. Simonyi Fund (Hungary), Department of Atomic Energy and Department of Science and Technology (India), Israel Science Foundation (Israel), Basic Science Research Program through NRF of the Ministry of Education (Korea), Physics Department, Lahore University of Management Sciences (Pakistan), Ministry of Education and Science, Russian Academy of Sciences, Federal Agency of Atomic Energy (Russia), VR and Wallenberg Foundation (Sweden), the U.S. Civilian Research and Development Foundation for the Independent States of the Former Soviet Union, the Hungarian American Enterprise Scholarship Fund, and the U.S.-Israel Binational Science Foundation.

APPENDIX: DATA TABLES

The asymmetry results are tabulated in Tables III and IV, while Tables V and VI list the systematic uncertainties from each source. Table VII gives the invariant cross section of muons from open heavy-flavor decays vs p_T.

TABLE III. Data table for A_N of muons from open heavy-flavor decays as a function of p_T.

	Forward ($x_F > 0$)				Backward ($x_F < 0$)			
Muon	p_T bin [GeV/c]	A_N	δA_N^{stat}	δA_N^{syst}	p_T bin [GeV/c]	A_N	δA_N^{stat}	δA_N^{syst}
μ^-	(1.25, 1.50)	−0.101	±0.088	$^{+0.047}_{-0.095}$	(1.25, 1.50)	−0.138	±0.086	$^{+0.061}_{-0.146}$
	(1.50, 2.00)	−0.003	±0.060	$^{+0.027}_{-0.027}$	(1.50, 2.00)	0.110	±0.060	$^{+0.084}_{-0.047}$
	(2.00, 2.50)	0.045	±0.077	$^{+0.034}_{-0.027}$	(2.00, 2.50)	−0.060	±0.076	$^{+0.034}_{-0.051}$
	(2.50, 3.00)	0.016	±0.077	$^{+0.017}_{-0.016}$	(2.50, 3.00)	0.022	±0.076	$^{+0.020}_{-0.019}$
	(3.00, 3.50)	−0.056	±0.094	$^{+0.014}_{-0.015}$	(3.00, 3.50)	−0.002	±0.093	$^{+0.014}_{-0.014}$
	(3.50, 5.00)	0.087	±0.104	$^{+0.028}_{-0.025}$	(3.50, 5.00)	0.018	±0.104	$^{+0.013}_{-0.013}$
μ^+	(1.25, 1.50)	0.030	±0.069	$^{+0.035}_{-0.035}$	(1.25, 1.50)	−0.004	±0.066	$^{+0.033}_{-0.033}$
	(1.50, 2.00)	−0.009	±0.040	$^{+0.026}_{-0.026}$	(1.50, 2.00)	−0.010	±0.039	$^{+0.025}_{-0.025}$
	(2.00, 2.50)	0.072	±0.055	$^{+0.036}_{-0.027}$	(2.00, 2.50)	−0.021	±0.054	$^{+0.025}_{-0.027}$
	(2.50, 3.00)	0.056	±0.065	$^{+0.028}_{-0.022}$	(2.50, 3.00)	−0.127	±0.066	$^{+0.034}_{-0.049}$
	(3.00, 3.50)	0.147	±0.087	$^{+0.038}_{-0.029}$	(3.00, 3.50)	−0.139	±0.088	$^{+0.033}_{-0.045}$
	(3.50, 5.00)	−0.104	±0.108	$^{+0.035}_{-0.046}$	(3.50, 5.00)	−0.054	±0.109	$^{+0.016}_{-0.016}$

TABLE IV. Data table for A_N of muons from open heavy-flavor decays as a function of x_F.

Muon	x_F bin	$\langle x_F \rangle$	A_N	δA_N^{stat}	δA_N^{syst}	Muon	x_F bin	$\langle x_F \rangle$	A_N	δA_N^{stat}	δA_N^{syst}
μ^-	$(-0.20, -0.05)$	-0.07	0.003	± 0.048	$^{+0.007}_{-0.013}$	μ^+	$(-0.20, -0.05)$	-0.07	-0.030	± 0.035	$^{+0.009}_{-0.014}$
	$(-0.05, 0.00)$	-0.04	-0.009	± 0.061	$^{+0.006}_{-0.010}$		$(-0.05, 0.00)$	-0.04	-0.026	± 0.043	$^{+0.009}_{-0.026}$
	(0.00, 0.05)	0.04	-0.030	± 0.062	$^{+0.010}_{-0.015}$		(0.00, 0.05)	0.04	-0.004	± 0.045	$^{+0.005}_{-0.013}$
	(0.05, 0.20)	0.07	0.019	± 0.047	$^{+0.009}_{-0.007}$		(0.05, 0.20)	0.07	0.058	± 0.035	$^{+0.023}_{-0.013}$

TABLE V. Sources of δA_N^{syst} for muons as a function of p_T.

		Forward ($x_F > 0$)					Backward ($x_F < 0$)			
Muon	p_T bin [GeV/c]	$\delta A_N^{\delta f_h}$	δA_N^{h}	$\delta A_N^{J/\psi \to \mu}$	$\delta A_N^{\text{method}}$	p_T bin [GeV/c]	$\delta A_N^{\delta f_h}$	δA_N^{h}	$\delta A_N^{J/\psi \to \mu}$	$\delta A_N^{\text{method}}$
μ^-	(1.25, 1.50)	$^{+0.036}_{-0.090}$	$^{+0.030}_{-0.030}$	$^{+0.001}_{-0.000}$	$^{+0.008}_{-0.008}$	(1.25, 1.50)	$^{+0.054}_{-0.143}$	$^{+0.030}_{-0.030}$	$^{+0.000}_{-0.000}$	$^{+0.003}_{-0.003}$
	(1.50, 2.00)	$^{+0.003}_{-0.001}$	$^{+0.026}_{-0.026}$	$^{+0.001}_{-0.001}$	$^{+0.004}_{-0.004}$	(1.50, 2.00)	$^{+0.079}_{-0.038}$	$^{+0.027}_{-0.027}$	$^{+0.001}_{-0.001}$	$^{+0.007}_{-0.007}$
	(2.00, 2.50)	$^{+0.024}_{-0.012}$	$^{+0.023}_{-0.023}$	$^{+0.003}_{-0.003}$	$^{+0.006}_{-0.006}$	(2.00, 2.50)	$^{+0.022}_{-0.044}$	$^{+0.023}_{-0.023}$	$^{+0.003}_{-0.003}$	$^{+0.010}_{-0.010}$
	(2.50, 3.00)	$^{+0.004}_{-0.004}$	$^{+0.014}_{-0.014}$	$^{+0.005}_{-0.003}$	$^{+0.007}_{-0.007}$	(2.50, 3.00)	$^{+0.009}_{-0.006}$	$^{+0.014}_{-0.014}$	$^{+0.004}_{-0.004}$	$^{+0.010}_{-0.010}$
	(3.00, 3.50)	$^{+0.008}_{-0.011}$	$^{+0.010}_{-0.010}$	$^{+0.005}_{-0.004}$	$^{+0.001}_{-0.001}$	(3.00, 3.50)	$^{+0.003}_{-0.004}$	$^{+0.010}_{-0.010}$	$^{+0.005}_{-0.005}$	$^{+0.008}_{-0.008}$
	(3.50, 5.00)	$^{+0.018}_{-0.014}$	$^{+0.009}_{-0.009}$	$^{+0.007}_{-0.005}$	$^{+0.019}_{-0.019}$	(3.50, 5.00)	$^{+0.001}_{-0.002}$	$^{+0.009}_{-0.009}$	$^{+0.006}_{-0.006}$	$^{+0.007}_{-0.007}$
μ^+	(1.25, 1.50)	$^{+0.007}_{-0.008}$	$^{+0.034}_{-0.034}$	$^{+0.000}_{-0.000}$	$^{+0.007}_{-0.007}$	(1.25, 1.50)	$^{+0.001}_{-0.001}$	$^{+0.032}_{-0.032}$	$^{+0.000}_{-0.000}$	$^{+0.001}_{-0.001}$
	(1.50, 2.00)	$^{+0.004}_{-0.007}$	$^{+0.025}_{-0.025}$	$^{+0.001}_{-0.001}$	$^{+0.001}_{-0.001}$	(1.50, 2.00)	$^{+0.001}_{-0.003}$	$^{+0.025}_{-0.025}$	$^{+0.001}_{-0.001}$	$^{+0.003}_{-0.003}$
	(2.00, 2.50)	$^{+0.028}_{-0.015}$	$^{+0.023}_{-0.023}$	$^{+0.003}_{-0.002}$	$^{+0.003}_{-0.003}$	(2.00, 2.50)	$^{+0.005}_{-0.011}$	$^{+0.022}_{-0.022}$	$^{+0.002}_{-0.002}$	$^{+0.011}_{-0.011}$
	(2.50, 3.00)	$^{+0.021}_{-0.014}$	$^{+0.017}_{-0.017}$	$^{+0.004}_{-0.003}$	$^{+0.006}_{-0.006}$	(2.50, 3.00)	$^{+0.029}_{-0.046}$	$^{+0.017}_{-0.017}$	$^{+0.003}_{-0.003}$	$^{+0.006}_{-0.006}$
	(3.00, 3.50)	$^{+0.035}_{-0.025}$	$^{+0.013}_{-0.013}$	$^{+0.005}_{-0.003}$	$^{+0.007}_{-0.007}$	(3.00, 3.50)	$^{+0.027}_{-0.041}$	$^{+0.013}_{-0.013}$	$^{+0.004}_{-0.004}$	$^{+0.012}_{-0.012}$
	(3.50, 5.00)	$^{+0.031}_{-0.043}$	$^{+0.013}_{-0.013}$	$^{+0.006}_{-0.004}$	$^{+0.008}_{-0.008}$	(3.50, 5.00)	$^{+0.004}_{-0.004}$	$^{+0.013}_{-0.013}$	$^{+0.005}_{-0.005}$	$^{+0.005}_{-0.005}$

TABLE VI. Sources of δA_N^{syst} for muons as a function of x_F.

Muon	x_F bin	$\delta A_N^{\delta f_h}$	$\delta A_N^{J/\psi \to \mu}$	$\delta A_N^{\text{method}}$	Muon	x_F bin	$\delta A_N^{\delta f_h}$	$\delta A_N^{J/\psi \to \mu}$	$\delta A_N^{\text{method}}$
μ^-	$(-0.20, -0.05)$	$^{+0.003}_{-0.012}$	$^{+0.005}_{-0.005}$	$^{+0.003}_{-0.003}$	μ^+	$(-0.20, -0.05)$	$^{+0.006}_{-0.013}$	$^{+0.004}_{-0.004}$	$^{+0.006}_{-0.006}$
	$(-0.05, 0.00)$	$^{+0.003}_{-0.008}$	$^{+0.001}_{-0.001}$	$^{+0.005}_{-0.005}$		$(-0.05, 0.00)$	$^{+0.009}_{-0.026}$	$^{+0.001}_{-0.001}$	$^{+0.002}_{-0.002}$
	(0.00, 0.05)	$^{+0.008}_{-0.013}$	$^{+0.001}_{-0.001}$	$^{+0.007}_{-0.007}$		(0.00, 0.05)	$^{+0.004}_{-0.013}$	$^{+0.001}_{-0.001}$	$^{+0.003}_{-0.003}$
	(0.05, 0.20)	$^{+0.005}_{-0.004}$	$^{+0.005}_{-0.004}$	$^{+0.005}_{-0.005}$		(0.05, 0.20)	$^{+0.022}_{-0.012}$	$^{+0.004}_{-0.003}$	$^{+0.005}_{-0.005}$

TABLE VII. Data table for the invariant cross section of muons from open heavy-flavor decays in $1.4 < |y| < 2.0$.

p_T [GeV/c]	$E\frac{d^2\sigma}{dp^3}$ [mb GeV^{-2}]	Stat uncert.	Syst uncert.	p_T [GeV/c]	$E\frac{d^2\sigma}{dp^3}$ [mb GeV^{-2}]	Stat uncert.	Syst uncert.
1.375	7.9×10^{-5}	9.4×10^{-7}	2.4×10^{-5}	3.25	3.1×10^{-7}	1.1×10^{-8}	4.5×10^{-8}
1.625	3.3×10^{-5}	3.7×10^{-7}	8.2×10^{-6}	3.75	9.8×10^{-8}	5.0×10^{-9}	1.4×10^{-8}
1.875	1.2×10^{-5}	1.8×10^{-7}	2.9×10^{-6}	4.25	3.2×10^{-8}	2.8×10^{-9}	4.7×10^{-9}
2.125	5.2×10^{-6}	1.0×10^{-7}	1.2×10^{-6}	4.75	1.7×10^{-8}	1.8×10^{-9}	2.4×10^{-9}
2.375	2.4×10^{-6}	5.9×10^{-8}	4.7×10^{-7}	5.5	4.5×10^{-9}	6.1×10^{-10}	6.5×10^{-10}
2.625	1.4×10^{-6}	3.8×10^{-8}	2.4×10^{-7}	6.5	1.1×10^{-9}	3.3×10^{-10}	2.0×10^{-10}
2.875	6.8×10^{-7}	2.6×10^{-8}	1.1×10^{-7}				

[1] R. D. Klem, J. E. Bowers, H. W. Courant, H. Kagan, M. L. Marshak, E. A. Peterson, K. Ruddick, W. H. Dragoset, and J. B. Roberts, Measurement of Asymmetries of Inclusive Pion Production in Proton Proton Interactions at 6 and 11.8 GeV/c, Phys. Rev. Lett. **36**, 929 (1976).

[2] G. L. Kane, J. Pumplin, and W. Repko, Transverse Quark Polarization in Large-p_T Reactions, e^+e^- Jets, and Leptoproduction: A Test of Quantum Chromodynamics, Phys. Rev. Lett. **41**, 1689 (1978).

[3] C. E. Allgower *et al.*, Measurement of analyzing powers of $\pi+$ and π^- produced on a hydrogen and a carbon target with a $22-\mathrm{GeV}/c$ incident polarized proton beam, Phys. Rev. D **65**, 092008 (2002).

[4] J. Antille, L. Dick, L. Madansky, D. Perret-Gallix, M. Werlen, A. Gonidec, K. Kuroda, and P. Kyberd, Spin dependence of the inclusive reaction $p+p$ (polarized) $\to \pi^0+X$ at 24 GeV/c for high-p_T π^0 produced in the central region, Phys. Lett. **94B**, 523 (1980).

[5] D. L. Adams *et al.* (FNAL-E581/E704 Collaboration), Comparison of spin asymmetries and cross sections in π^0 production by 200 GeV polarized antiprotons and protons, Phys. Lett. B **261**, 201 (1991).

[6] D. L. Adams *et al.* (FNAL-E704 Collaboration), Analyzing power in inclusive π^+ and π^- production at high x_F with a 200 GeV polarized proton beam, Phys. Lett. B **264**, 462 (1991).

[7] I. Arsene *et al.* (BRAHMS Collaboration), Single Transverse Spin Asymmetries of Identified Charged Hadrons in Polarized pp Collisions at $\sqrt{s}=62.4$ GeV, Phys. Rev. Lett. **101**, 042001 (2008).

[8] John Adams *et al.* (STAR Collaboration), Cross Sections and Transverse Single-Spin Asymmetries in Forward Neutral-Pion Production from Proton Collisions at $\sqrt{s}=200$ GeV, Phys. Rev. Lett. **92**, 171801 (2004).

[9] B. I. Abelev *et al.* (STAR Collaboration), Forward Neutral-Pion Transverse Single-Spin Asymmetries in $p+p$ Collisions at $\sqrt{s}=200$ GeV, Phys. Rev. Lett. **101**, 222001 (2008).

[10] M. M. Mondal (STAR Collaboration), Measurement of the transverse single-spin asymmetries for π^0 and jet-like events at forward rapidities at STAR in $p+p$ collisions at $\sqrt{s}=500$ GeV, *Proc. Sci.*, DIS20142014 (2014) 216.

[11] H. Jung, D. Treleani, M. Strikman, and N. van Buuren, Preview from RHIC Run 15 pp and p Au forward neutral pion production from transversely polarized protons, in *Proceedings of the 7th International Workshop on Multiple Partonic Interactions at the LHC (MPI@LHC 2015), Miramare, Trieste, Italy* (2016), pp. 1–259.

[12] A. Adare *et al.* (PHENIX Collaboration), Measurement of transverse-single-spin asymmetries for midrapidity and forward-rapidity production of hadrons in polarized $p+p$ collisions at $\sqrt{s}=200$ and 62.4 GeV, Phys. Rev. D **90**, 012006 (2014).

[13] A. Adare *et al.* (PHENIX Collaboration), Cross section and transverse single-spin asymmetry of η mesons in $p^\uparrow+p$ collisions at $\sqrt{s}=200$ GeV at forward rapidity, Phys. Rev. D **90**, 072008 (2014).

[14] L. Adamczyk *et al.* (STAR Collaboration), Transverse single-spin asymmetry and cross-section for π^0 and η mesons at large Feynman-x in polarized $p+p$ collisions at $\sqrt{s}=200$ GeV, Phys. Rev. D **86**, 051101 (2012).

[15] D. W. Sivers, Single spin production asymmetries from the hard scattering of point-like constituents, Phys. Rev. D **41**, 83 (1990).

[16] D. W. Sivers, Hard scattering scaling laws for single spin production asymmetries, Phys. Rev. D **43**, 261 (1991).

[17] John C. Collins, Fragmentation of transversely polarized quarks probed in transverse momentum distributions, Nucl. Phys. **B396**, 161 (1993).

[18] A. Airapetian *et al.* (HERMES Collaboration), Effects of transversity in deep-inelastic scattering by polarized protons, Phys. Lett. B **693**, 11 (2010).

[19] C. Adolph *et al.* (COMPASS Collaboration), Experimental investigation of transverse spin asymmetries in μ-p SIDIS processes: Collins asymmetries, Phys. Lett. B **717**, 376 (2012).

[20] Ted C. Rogers and Piet J. Mulders, No generalized TMD-factorization in hadro-production of high transverse momentum hadrons, Phys. Rev. D **81**, 094006 (2010).

[21] A. V. Efremov and O. V. Teryaev, QCD asymmetry and polarized hadron structure functions, Phys. Lett. B **150B**, 383 (1985).

[22] J.-W. Qiu and G. F. Sterman, Single Transverse Spin Asymmetries, Phys. Rev. Lett. **67**, 2264 (1991).

[23] E. Norrbin and T. Sjöstrand, Production and hadronization of heavy quarks, Eur. Phys. J. C **17**, 137 (2000).

[24] A. Adare *et al.* (PHENIX Collaboration), Measurement of transverse single-spin asymmetries for J/ψ production in polarized $p+p$ collisions at $\sqrt{s}=200$ GeV, Phys. Rev. D **82**, 112008 (2010); Erratum, Phys. Rev. D **86**, 099904 (2012).

[25] F. Yuan, Heavy quarkonium production in single transverse polarized high energy scattering, Phys. Rev. D **78**, 014024 (2008).

[26] A. Adare *et al.* (PHENIX Collaboration), Ground and excited charmonium state production in $p+p$ collisions at $\sqrt{s}=200$ GeV, Phys. Rev. D **85**, 092004 (2012).

[27] Y. Koike and S. Yoshida, Probing the three-gluon correlation functions by the single spin asymmetry in $p^\uparrow p \to DX$, Phys. Rev. D **84**, 014026 (2011).

[28] Z.-B. Kang, J.-W. Qiu, W. Vogelsang, and F. Yuan, Accessing tri-gluon correlations in the nucleon via the single spin asymmetry in open charm production, Phys. Rev. D **78**, 114013 (2008).

[29] S. J. Brodsky, F. Fleuret, C. Hadjidakis, and J. P. Lansberg, Physics opportunities of a fixed-target experiment using the LHC beams, Phys. Rep. **522**, 239 (2013).

[30] K. Adcox *et al.* (PHENIX Collaboration), PHENIX detector overview, Nucl. Instrum. Methods Phys. Res., Sect. A **499**, 469 (2003).

[31] H. Akikawa *et al.* (PHENIX Collaboration), PHENIX muon arms, Nucl. Instrum. Methods Phys. Res., Sect. A **499**, 537 (2003).

[32] S. Adachi *et al.*, Trigger electronics upgrade of PHENIX muon tracker, Nucl. Instrum. Methods Phys. Res., Sect. A **703**, 114 (2013).

[33] M. Allen *et al.* (PHENIX Collaboration), PHENIX inner detectors, Nucl. Instrum. Methods Phys. Res., Sect. A **499**, 549 (2003).

[34] H. Okada *et al.*, Measurement of the analyzing power in pp elastic scattering in the peak CNI region at RHIC, Phys. Lett. B **638**, 450 (2006).

[35] I. Nakagawa *et al.*, p-carbon polarimetry at RHIC, AIP Conf. Proc. **980**, 380 (2008).
[36] H. Huang and K. Kurita, Fiddling carbon strings with polarized proton beams, AIP Conf. Proc. **868**, 3 (2006).
[37] S. S. Adler *et al.* (PHENIX Collaboration), Mid-Rapidity Neutral Pion Production in Proton-Proton Collisions at $\sqrt{s} = 200$ GeV, Phys. Rev. Lett. **91**, 241803 (2003).
[38] K. A. Drees, Z. Xu, B. Fox, and H. Huang, Results from Vernier scans at RHIC during the pp Run 2001–2002, in *Proceedings of the PAC2003 Conference, Portland* (IEEE, Piscataway, 2003), p. 1688.
[39] A. Adare *et al.* (PHENIX Collaboration), Nuclear-modification factor for open-heavy-flavor production at forward rapidity in Cu + Cu collisions at $\sqrt{s_{NN}} = 200$ GeV, Phys. Rev. C **86**, 024909 (2012).
[40] A. Adare *et al.* (PHENIX Collaboration), Cold-Nuclear-Matter Effects on Heavy-Quark Production at Forward and Backward Rapidity in $d + \mathrm{Au}$ Collisions at $\sqrt{s_{NN}} = 200$ GeV, Phys. Rev. Lett. **112**, 252301 (2014).
[41] S. Agostinelli *et al.* (GEANT4 Collaboration), GEANT4: A simulation toolkit, Nucl. Instrum. Methods Phys. Res., Sect. A **506**, 250 (2003).
[42] A. Adare *et al.* (PHENIX Collaboration), Heavy quark production in $p + p$ and energy loss and flow of heavy quarks in Au + Au collisions at $\sqrt{s_{NN}} = 200$ GeV, Phys. Rev. C **84**, 044905 (2011).
[43] A. Adare *et al.* (PHENIX Collaboration), Identified charged hadron production in $p + p$ collisions at $\sqrt{s} = 200$ and 62.4 GeV, Phys. Rev. C **83**, 064903 (2011).
[44] G. Agakishiev *et al.* (STAR Collaboration), Identified Hadron Compositions in $p + p$ and Au + Au Collisions at High Transverse Momenta at $\sqrt{s_{NN}} = 200$ GeV, Phys. Rev. Lett. **108**, 072302 (2012).
[45] T. Sjöstrand, S. Mrenna, and P. Z. Skands, PYTHIA 6.4 Physics and Manual, J. High Energy Phys. 05 (2006) 026.
[46] C. Aidala *et al.* (PHENIX Collaboration), B-meson production at forward and backward rapidity in $p + p$ and Cu + Au collisions at $\sqrt{s_{NN}} = 200$ GeV, arXiv:1702.01085.
[47] M. Cacciari, M. Greco, and P. Nason, The p_T spectrum in heavy flavor hadroproduction, J. High Energy Phys. 05 (1998) 007.
[48] H. Fujii and K. Watanabe, Leptons from heavy-quark semileptonic decay in pA collisions within the CGC framework, Nucl. Phys. **A951**, 45 (2016).
[49] T. Sjöstrand, S. Ask, J. R. Christiansen, R. Corke, N. Desai, P. Ilten, S. Mrenna, S. Prestel, C. O. Rasmussen, and P. Z. Skands, An introduction to PYTHIA 8.2, Comput. Phys. Commun. **191**, 159 (2015).